Low-Loss and Weakly Coupled Eight-Mode Nodeless Hollow-Core Anti-Resonant Fiber With Three-Layer Nested Tubes in Each Cladding Unit

Biao Wang, Wei Gao, Xin Wang, Paul K. Chu, *Fellow, IEEE*, and Shuqin Lou

***Abstract*—A low-loss and weakly coupled eight-mode nodeless hollow-core anti-resonant fiber (HC-ARF) is designed and analyzed. The cladding structure comprising six cladding units with three-layer nested tubes suppresses mode coupling between the eight core modes (LP_{01}-LP_{31a}, LP_{31b}-LP_{41}) and cladding modes. By optimizing the core radius and nested tubes, the confinement losses of the LP_{01}-LP_{41} modes can be controlled to be below 1.72×10^{-4} dB/m. The effective refractive index difference between adjacent core modes is greater than 1.0×10^{-4}, and the corresponding differential mode group delay is larger than 0.38 ps/m in the wavelength range between 1480 nm and 1670 nm. As a result, weak coupling can be accomplished between LP_{01}-LP_{41}, and these eight core modes can propagate through the HC-ARF with similar low losses. Numerical analysis demonstrates that the eight weakly coupled modes can be stably supported at a bending radius of 20 cm. At smaller bending radii of 5 and 3 cm, five and two weakly coupled core modes, respectively, can still be supported.**

***Index Terms*—Anti-resonant fiber, few-mode fiber, hollow core fiber, microstructured fiber, optical fiber design.**

I. Introduction

ALTHOUGH the space division multiplexing (SDM) technology based on solid-core fibers can improve the transmission capacity of communication systems [1], [2], [3], [4], the transmission capacity is still limited by the nonlinearity of solid-core fibers [5], [6]. Hollow core fibers (HCFs), which can propagate light signals through the air core, offer unique advantages, such as small delay, low nonlinear, little loss, and wide transmission bandwidth, which can overcome the limitations of conventional solid core fibers and increase the transmission capacity in optical fiber communication [7]. For example, SDM based on HCFs can increase the transmission capacity by orders of magnitude and may be able to overcome the capacity bottleneck of optical communication systems. The loss of a hollow-core anti-resonant fiber (HC-ARF) has been reduced to 0.11 dB/km [8], which is already lower than that of the commercial standard single-mode fiber (SMF). Compared to the hollow-core photonic bandgap fiber (HC-PBGF) [9], [10] and Kagome fiber [11], the HC-ARF has a simpler and more flexible structure, lower loss, wider transmission bandwidth, and easier fabrication. Owing to the small overlap in the light field with the host materials, the HC-ARF can suppress the surface mode and reduce surface scattering loss (SSL) [12], [13], [14]. Consequently, the confinement loss (CL) and bending loss (BL) are the dominant losses of HC-ARFs [15].

Generally, HC-ARFs can propagate the fundamental mode (FM) and multiple high-order modes (HOMs) at the same time. In single-mode operation, it is common to utilize phase matching between HOMs and cladding modes to realize the coupling of HOMs with the cladding mode, causing a significant increase in the loss of the HOMs and suppression of the HOMs [16]. In fact, the structure of the HC-ARF can be modulated to deliberately break the phase matching between the HOMs in the core and cladding modes. As a result, the HC-ARF can support the propagation of not only low-loss FM but also low-loss multiple HOMs (mode group) to increase the spatial mode density and realize the SDM of modes. In multi-mode fiber transmission systems, the combination of multimode into a single channel is a common practice [17]. Currently, multi-mode HC-ARFs has the potential for high-power laser delivery [18], [19], [20]. Compared with the reported multi-mode HC-ARFs, few-mode HC-ARFs can effectively control intermode crosstalk, allowing each mode to potentially function as an independent data channel. Similar to solid core fibers, there are two possible ways to implement mode division multiplexing in HC-ARFs, including the design of few-mode HC-ARF with low differential mode group delay (DMGD) or with weakly coupled few-mode propagation. Low DMGD fibers allow arbitrary mixing between the spatial modes of the core and compensate for the crosstalk between the modes using a multiple-input multiple-output digital signal processing technique (MIMO-DSP) at the receiving end. It has been shown that the HC-ARFs can guide seven mode groups in the core with a relatively low differential loss in the wavelength range between 850 nm and 1050 nm [21]. However, this approach suffers from the high DMGD and may require the use of complex MIMO-DSP algorithms on the receiver side. Consequently,

Received 28 August 2024; revised 11 November 2024; accepted 23 November 2024. Date of publication 27 November 2024; date of current version 17 March 2025. This work was supported in part by the National Natural Science Foundation of China under Grant 12174022 and in part by Beijing Municipal Natural Science Foundation under Grant 1232028. *(Corresponding author: Shuqin Lou.)*

Biao Wang, Wei Gao, Xin Wang, and Shuqin Lou are with the Key Laboratory of Communication and Information Systems, Beijing Municipal Commission of Education, School of Electronic and Information Engineering, Beijing Jiaotong University, Beijing 100044, China (e-mail: b.wang@bjtu.edu.cn; 23111026@bjtu.edu.cn; xin.wang@bjtu.edu.cn; shqlou@bjtu.edu.cn).

Paul K. Chu is with the Department of Physics, Department of Materials Science & Engineering, and Department of Biomedical Engineering, City University of Hong Kong, Hong Kong (e-mail: paul.chu@cityu.edu.hk).

Color versions of one or more figures in this article are available at https://doi.org/10.1109/JLT.2024.3507111.

Digital Object Identifier 10.1109/JLT.2024.3507111

it is difficult to determine the reliability of large-scale and long-distance data transmission in addition to the cost issue. Weakly coupled fibers reduce the negative effects of crosstalk by increasing the effective refractive index difference Δn_{eff} between modes. When $\Delta n_{\text{eff}} > 10^{-4}$ between core modes, the energy coupling between the core modes can be reduced [22], and the signal is detected directly or by using low-dimensional MIMO-DSP on the receiver side. This approach is suitable, for example, for short-range information transmission for data centers, where there is an urgent need to reduce the complexity of MIMO. Wang et al. have designed a weakly coupled HC-ARF for transmission of the LP_{01} and LP_{11} modes in the wavelength range from 1.31 μm to 1.65 μm. Both modes have low CLs of less than 1.0×10^{-2} dB/m and a large effective refractive index difference Δn_{eff} greater than 5.0×10^{-4}. Moreover, the bending radius can be decreased to 10 cm [23]. Liu et al. have reduced the CL of the weakly coupled few-mode HC-ARF using conjoined nested tubes as the cladding units. It can support five modes, including the LP_{01}-LP_{31} modes from 1.40 μm to 1.61 μm. The CLs of all five modes are lower than 3.0×10^{-4} dB/m, thereby keeping the effective refractive index difference Δn_{eff} between the HOMs greater than 1.0×10^{-4}. The bending resistance improves, and the permissible bending radius is reduced to 6 cm [24].

In this work, a weakly coupled nodeless HC-ARF that can support the propagation of eight modes, including LP_{01}, LP_{11}, LP_{21}, LP_{02}, LP_{31a}, LP_{31b}, $LP_{12,}$ and LP_{41} modes, is designed and analyzed. The cladding structure consists of six cladding units with three-layer nested tubes to suppress mode coupling between the eight core modes LP_{01}-LP_{41} and cladding modes. Therefore, the CLs of LP_{01}-LP_{41} modes can be reduced. By optimizing the size of the core and nested tubes, the CLs of the LP_{01}-LP_{41} modes are less than 1.72×10^{-4} dB/m between 1480 nm and 1670 nm. In addition, Δn_{eff} between adjacent core modes is greater than 1.0×10^{-4}, and the corresponding differential mode group delay is larger than 0.38 ps/m.

II. Fiber Structure

The ARF consists of an air core with a radius R, N nodeless cladding units with a gap g, and an outer silica jacket layer, as shown in Fig. 1. Each cladding unit comprises three-layer nested tubes, where the outer tube and middle tube are concentric circular tubes with radii of r_1 and r_2. Solid silica rods are the support for these two tubes. The inner nested structure consists of two small circular tubes with the same radius, r_3, arranged symmetrically on either side of the center of the circle and internally tangent to the middle-nested tube. Acting as Fabry-Perot resonators in the radial direction, the three-layer nested tubes provide more effective reflections to the expected core modes. Therefore, the confinement losses of the expected core modes can be reduced to realize few-mode transmission. The nested tubes in the cladding have the same wall thickness, t, which is determined by the anti-resonant reflection condition [16]:

$$t = \frac{\lambda(m - 0.5)}{2\sqrt{n^2 - 1}}. \tag{1}$$

II. Fiber Structure

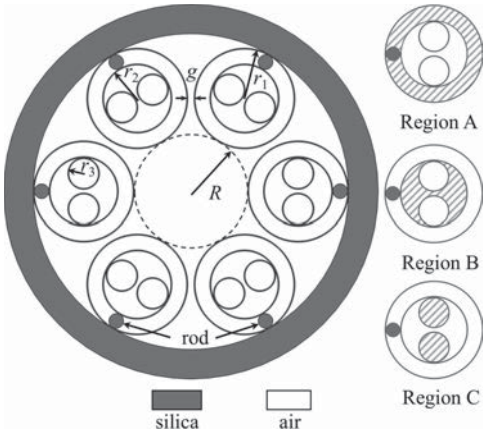

Fig. 1. Cross-section of eight-mode nodeless HC-ARF with three-layer nested tubes in each cladding unit and three air regions designated as Region A, Region B, and Region C in each cladding unit.

where λ is the light wavelength in vacuum, n is the silica refractive index, and m represents the order of the antiresonance ($m = 1, 2, 3, \cdots$). The unique nesting structure enhances the degree of freedom of partition of the cladding unit, leading to a reduction in the effective refractive index of cladding modes. This can effectively suppresses the phase matched coupling between cladding modes and core modes, thereby the number of low loss core modes can be efficiently increased. Each cladding unit can be divided into three air regions, namely region A, region B, and region C, as shown by the shadow area in Fig. 1. The cladding modes are mainly distributed in these three regions.

In terms of the geometric relationship, the radius of the outer cladding tube r_1 should satisfy the following equation:

$$r_1 = \frac{g/2 + t - (R + t)\sin(\pi/N)}{\sin(\pi/N) - 1}. \tag{2}$$

Considering the structure with three-layer nested tubes, we use the relative structural parameters r_2/r_1 and r_3/r_2 in the following analysis. By selecting the relative structural parameters r_2/r_1 and r_3/r_2, the mode characteristics of the cladding units can be tailored to suppress the coupling between the expected core HOMs and cladding modes in order to support few-mode propagation in the HC-ARF.

The initial structural parameters are set as $N = 6$, $g = 1.5$ μm, $r_2/r_1 = 0.60$, $r_3/r_2 = 0.44$, and $R = 23$ μm. In order to obtain a wide transmission bandwidth, the wall thickness of the cladding tubes is set as $t = 0.46$ μm so as to operate in the first-order anti-resonance band. The mode properties of the few-mode HC-ARF are simulated by the finite element method combined with the perfectly matched layer (PML) as the boundary condition. In order to ensure simulation accuracy, the mesh sizes in the air and silica regions are set as $\lambda/4$ and $\lambda/6$, respectively [25]. A PML is set outside the cladding layer with a thickness of 8 μm and a mesh size of λ. In the simulation, the refractive index of air is 1 and that of silica is determined by the Sellmeier equation [26]. Fig. 2 shows the electric field distribution, n_{eff}, and confinement loss (CL) of the first eight core modes at 1550 nm. The CL is

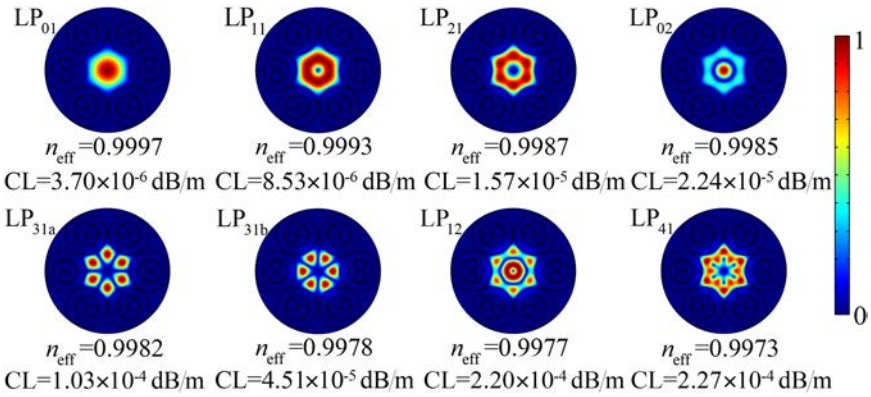

Fig. 2. Electric field distribution, n_{eff}, and CL of the first eight core modes at $\lambda = 1550$ nm of the HC-ARF for $N = 6$, $g = 1.50$ μm, $r_2/r_1 = 0.60$, $r_3/r_2 = 0.44$, and $R = 23$ μm.

calculated by the following equation [27]:

$$\mathrm{CL} = \frac{20}{\ln 10}\frac{2\pi}{\lambda}\mathrm{Im}\left(n_{\text{eff}}\right). \tag{3}$$

where Im(n_{eff}) is the imaginary part of the effective refractive index n_{eff} of the mode. Fig. 2 shows that the first eight core modes from LP_{01} to LP_{41} modes are confined in the fiber core, and the CLs are less than 2.27×10^{-4} dB/m. Moreover, Δn_{eff} between adjacent core modes is greater than 1.3×10^{-4} and can satisfy the weak coupling condition and reduce the crosstalk between these modes [22]. We define the ratio of the CL of HOM to that of LP_{01} mode as CLR. The CLRs of the seven core HOMs, that is, LP_{11}-LP_{41} modes, can be calculated according to Fig. 2. The CLRs of the seven core HOMs are less than 62, implying that these eight core modes can be propagated stably.

III. Optimization for Eight LP_{01} -LP_{41} Modes

The three-layer nested cladding unit and core size play a crucial role in regulating the mode characteristics. This section delves into and determines the impact of key parameters on the characteristics of the few-mode HC-ARF.

A. Effect of Cladding Unit Number

Firstly, we investigate the effect of the number of cladding units N on the CLs and CLRs of LP_{01}-LP_{41} modes in the HC-ARF. The number of cladding units N directly affect the dimensions of the cladding units. When all initial parameters except N keep constant, the effect of the number of cladding units N on CLs and CLRs of LP_{01}-LP_{41} modes is depicted in Fig. 3. It can be clearly seen that the CLs and CLRs of LP_{01}-LP_{41} modes basically appear a decreasing trend when the number of cladding units is increased from $N = 5$ to $N = 7$. This is due to the fact that a decrease in the number of cladding units would lead to an increase in the hollow region within the cladding units, which results in core modes more susceptible to be coupled with cladding modes and thus CLs of core mode increase. When N is 5, there is a significant increase in the CLs and CLRs of LP_{31a}-LP_{41} modes, in which the CLs of these modes are all greater than 10^{-2} dB/m order and the CLRs are all higher than 100. In order to maintain eight efficient propagation modes

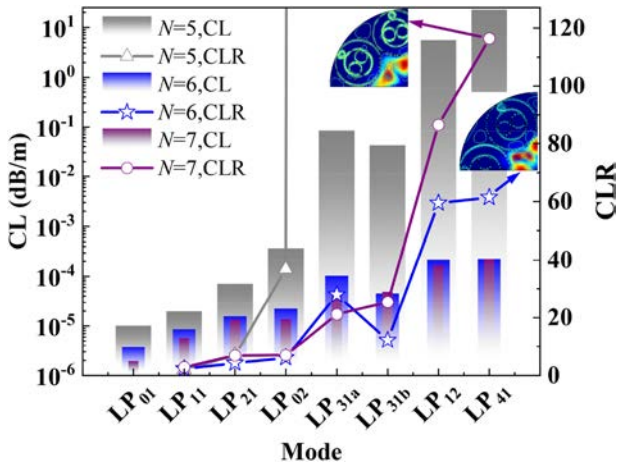

Fig. 3. Effect of the N on CLs and CLRs of the LP_{01}-LP_{41} modes of the HC-ARF for $g = 1.50$ μm, $r_2/r_1 = 0.60$, $r_3/r_2 = 0.44$, and $R = 23$ μm at 1550 nm. The insets depict the contours of the y-component of the electric field of LP_{41} mode at $N =$ of 6 and 7.

(LP_{01}-LP_{41} modes) in the HC-ARF, the number of cladding units N should be more than 5. For the case of $N = 6$ and $N = 7$, the CLs of LP_{11}-LP_{41} modes are all below 2.27×10^{-4} dB/m. But the CLRs of LP_{11}-LP_{41} modes except LP_{31a} at $N = 7$ are all higher than those at $N = 6$. For instance, the CLR of the LP_{41} mode is 116.36 at $N = 7$ and 61.38 at $N = 6$. This can be attributed to the increased overlap of the LP_{41} mode field with silica rods and silica walls due to small cladding units at $N = 7$, which can be clearly observed from the contour plot of y-component electric field in the insets of Fig. 3. So do the other propagation modes. In addition, the CLR of LP_{31a} at $N = 6$ is slightly higher than that at $N = 7$. Considering the effect of the cladding unit number on the CLs and CLRs of LP_{11}-LP_{41} modes, we choose the cladding unit number $N = 6$ in the following analysis.

B. Effect of Gap Between Cladding Units

Adjusting the gap g between the cladding units will also result in modifications to the overall dimensions of the entire cladding unit due to the fixed core size. Fig. 4 shows the effect of the gap g on the mode characteristics of the few-mode HC-ARF.

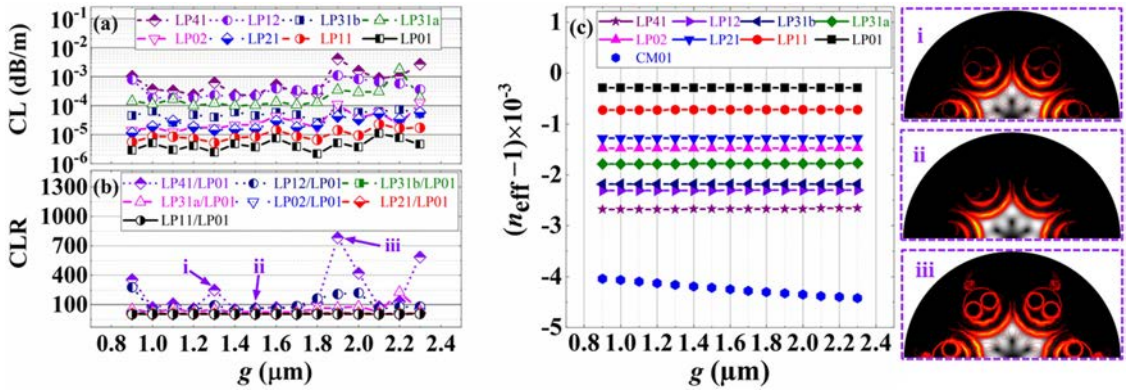

Fig. 4. Effect of the gap g between cladding units on (a) CLs, (b) CLRs of the LP_{01}-LP_{41} modes, and (c) n_{eff} curves of the LP_{01}-LP_{41} modes and cladding CM_{01} mode for the HC-ARF with $N = 6$, $r_2 / r_1 = 0.60$, $r_3 / r_2 = 0.44$, and $R = 23$ μm at 1550 nm. The rightest figures labeled i, ii, iii correspond to the points marked as i, ii, iii in (b) where the white regions and the red regions represent the electric field distribution and y-component of the Poynting vector of the LP_{41} mode, respectively.

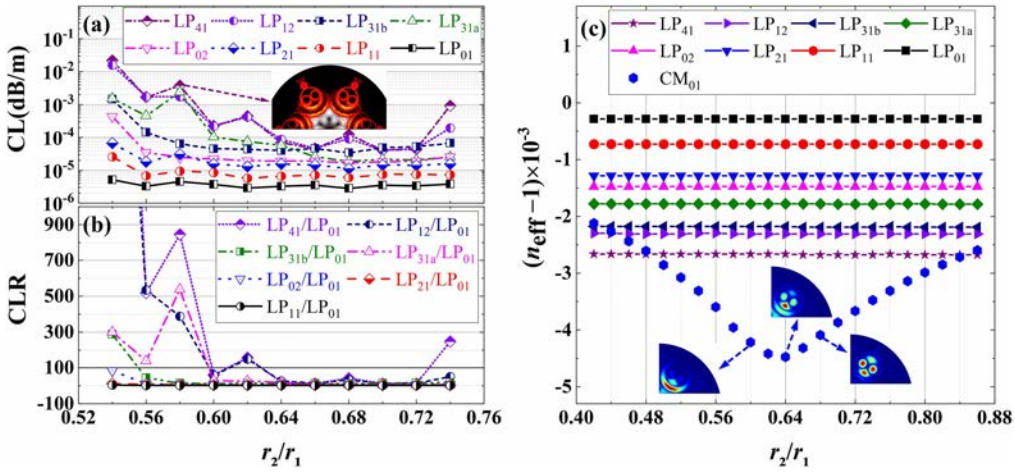

Fig. 5. Effects of the radius of the middle nested tube on (a) CLs and (b) CLRs of the LP_{01}-LP_{41} modes; (c) n_{eff} curves of the LP_{01}-LP_{41} modes and cladding CM_{01} mode of the HC-ARF for $N = 6$, $g = 1.50$ μm, $r_3 / r_2 = 0.44$, and $R = 23$ μm at 1550 nm. The electric field distribution of the LP_{41} mode (white) and the y-component of the Poynting vector (red) are shown in the inset in (a), and the electric field distribution of the CM_{01} mode is displayed in the insets in (c).

When g is varied between 1.40 μm and 1.70 μm, the CLs of the LP_{01}-LP_{41} modes are all below 5.29×10^{-4} dB/m, as shown in Fig. 4(a). Meanwhile, the CLRs of the LP_{11}-LP_{41} modes are all less than 86, as shown in Fig. 4(b). The neff curves of the LP01-LP41 modes and cladding fundamental mode (CM01) in Fig. 4(c) reveal that there is no crossing point between the LP_{01}-LP_{41} modes and CM_{01} mode and thus phase matching conditions between them are not satisfied, which means that the mode coupling between the eight core modes and cladding mode can be efficiently suppressed and low CLs can be achieved for the eight core modes. When $g < 1.40$ μm and $g > 1.70$ μm, there are some fluctuations in the CLs and CLRs for some high order core modes such as LP_{12}, LP_{31a}, and LP_{41} modes. This can be analyzed from the electric field distribution (white region) and y-component of the Poynting vector (red region) of LP_{41} mode in the rightest picture of Fig. 4 corresponding to points i, ii, and iii in Fig. 4(b). Compared with the figure i, figure ii illustrates that energy coupling from these core modes to the middle and inner tubes wall in the cladding can be enhanced when the g is reduced below 1.40 μm. Meanwhile, when g is increased to above 1.70 μm, figure iii demonstrates that energy coupling can be further expanded from these core modes to the silica rod and thus both CLs and CLRs appear a relatively high fluctuation. The n_{eff} of the cladding fundamental mode (CM_{01}) decreases as g increases, while the n_{eff} of the LP_{01}-LP_{41} mode remains nearly constant due to the constant core size, as can be seen from Fig. 4(c). Hence, g is set between 1.40 μm and 1.70 μm. When $g = 1.50$ μm, all LP_{01}-LP_{41} modes have low CLs below 2.27×10^{-4} dB/m and CLRs less than 59.45. Therefore, g is chosen as 1.50 μm for the following discussion.

C. Effects of Middle Nested Tube

As shown in Fig. 5, when r_2 / r_1 is varied between 0.64 and 0.72, the CLs of the LP_{01}-LP_{41} modes are below 1.22×10^{-4} dB/m. At the same time, the CLRs of the LP_{11}-LP_{41} modes are less than 50, indicating that the eight core modes have similar low CLs. The n_{eff} curves of the LP_{01}-LP_{41} modes and CM_{01} mode

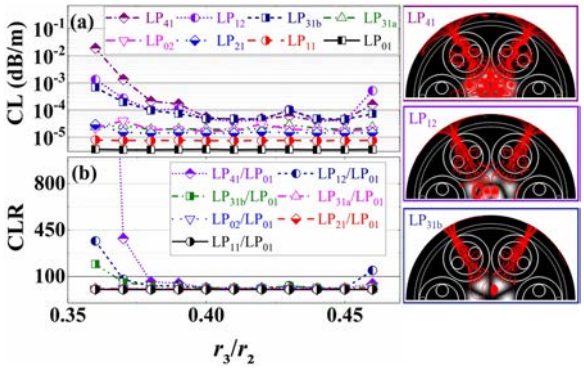

Fig. 6. Effects of the radius of the inner nested tube on (a) CLs and (b) CLRs of the LP_{01}-LP_{41} modes of the HC-ARF for $N = 6$, $g = 1.50$ μm, $r_2 / r_1 = 0.70$, and $R = 23$ μm at 1550 nm. The electric field distribution (white) and the transverse power flow (red) of the LP_{41} mode, LP_{12} mode, and LP_{31b} mode are shown in the insets on right for $r_3 / r_2 = 0.36$.

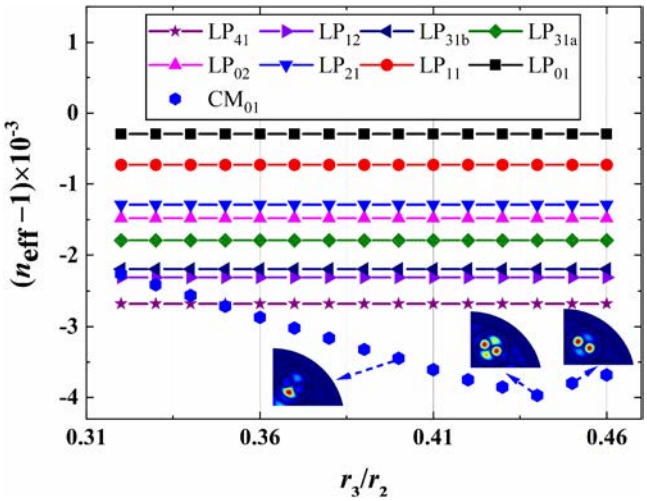

Fig. 7. Effects of the radius of the inner nested tube on n_{eff} of the LP_{01}-LP_{41} modes and cladding CM_{01} mode for $N = 6$, $g = 1.50$ μm, $r_2 / r_1 = 0.70$, and $R = 23$ μm at 1550 nm.

do not cross each other, meaning that mode coupling between LP_{01}-LP_{41} modes and cladding modes is suppressed. When $r_2 / r_1 < 0.60$, the CLs of the LP_{31a}, LP_{12}, and LP_{41} modes increase, and the CLRs of these modes increase dramatically, as shown in Fig. 5(a) and (b). This is caused by the strong coupling of the energy of these core modes with the middle tube, inner tube, and silica rod in the cladding, as shown in the inset in Fig. 5(a). Similarly, when $r_2 / r_1 > 0.72$, the LP_{12} and LP_{41} modes begin to couple to the silica layer in the cladding, and therefore, CLs increase. When $r_2 / r_1 < 0.50$, the n_{eff} of the CM_{01} mode in regions A and B increases with increasing region A until it is geometrically limited, and the n_{eff} curve will intersect those of the LP_{41}-LP_{01} modes in sequence. Similarly, when $r_2 / r_1 > 0.82$, the n_{eff} of the CM_{01} mode in regions B and C increases with the increase of these two regions until it is geometrically limited, and the n_{eff} curve intersects those of the LP_{41}-LP_{01} modes in sequence. At this time, the coupling of the energy of LP_{01}-LP_{41} modes to the silica layer and cladding modes strengthens, and the losses of these core modes increase. It is worth noting that the smallest n_{eff} of the CM_{01} mode appears at $r_2 / r_1 = 0.64$, which is away from the n_{eff} curves of the LP_{41}-LP_{01} modes. At this time, the modal field of the CM_{01} mode is mainly distributed in regions A, B, and C. When $r_2 / r_1 = 0.70$, the LP_{01}-LP_{41} modes have low CLs of less than 4.82×10^{-5} dB/m, and CLRs are less than 13.80. Therefore, r_2 / r_1 is chosen to be 0.70 for the following discussion.

D. Effects of Inner Nested Tubes

Fig. 6 shows that when r_3 / r_2 changes in the range from 0.38 to 0.45, the CLs of LP_{01}-LP_{41} modes are all below 2.11×10^{-4} dB/m, while the CLRs of LP_{11}-LP_{41} modes do not exceed 60.49. However, when $r_3 / r_2 < 0.38$, the CLs of the LP_{31b}, LP_{12}, and LP_{41} modes increase, and so do the corresponding CLRs, because the confinement ability of the two inner nested tubes becomes weaker when $r_3 / r_2 < 0.38$. Hence, the energy of the LP_{31b}, LP_{12}, and LP_{41} modes produces leakage through the gap between the two tubes in region B, as shown by the transverse power flow in the right inset in Fig. 6. The n_{eff} curves in Fig. 7 show that the CM_{01} mode approaches the core modes and intersects the LP_{41}-LP_{01} modes when $r_3 / r_2 < 0.36$. The high losses may stem from energy leakage of the LP_{01}-LP_{41} modes and coupling between the LP_{01}-LP_{41} modes and cladding modes. When $r_3 / r_2 > 0.45$, the CLs of the LP_{31b}, LP_{12}, and LP_{41} modes increase as the size of the inner nested tubes increases because the gradual proximity of the dielectric walls of the two inner nested tubes couples the mode energy to the silica layer and increases CL. The CM_{01} mode is distributed in both regions B and C when $r_3 / r_2 = 0.44$, where it has the smallest n_{eff}, away from the n_{eff} of LP_{41}-LP_{01} modes. When $r_3 / r_2 = 0.40$, the coupling between the cladding mode and the expected core modes is suppressed. It also ensures that the inner nested tube provides effective constraints to the eight core modes, and the LP_{01}-LP_{41} modes have similarly low CLs. Therefore, in the following discussion, r_3 / r_2 is chosen to be 0.40.

E. Effects of Core Size

Fig. 8 shows the effects of the core size on the mode characteristics of the few-mode HC-ARF. When the core size R changes between 19 μm and 26 μm, the CLs of the eight modes decrease with increasing core size, and the CLs of LP_{01}-LP_{41} modes are below 7.61×10^{-4} dB/m, as shown in Fig. 8(a). Meanwhile, the CLRs of the LP_{11}-LP_{41} modes are less than 48.45 except for $R = 24$ μm. When $R = 24$ μm, the CLR of the LP_{12} mode is greater than 100 because the energy of the LP_{12} mode is coupled to the middle tube, inner tube, and silica rod, as shown in the inset in Fig. 8(b). The n_{eff} curves of the LP_{01}-LP_{41} modes and CM_{01} mode in Fig. 8(c) reveal that there is no crossing between the LP_{01}-LP_{41} modes and CM_{01} mode, implying that the mode coupling between the eight core modes and cladding modes is suppressed to generate low CLs for the eight core modes. The Δn_{eff} values between adjacent core modes are all greater than 1.0×10^{-4}, as shown in Fig. 8(d), indicative of suppression of crosstalk between adjacent core modes. However, when $R >$

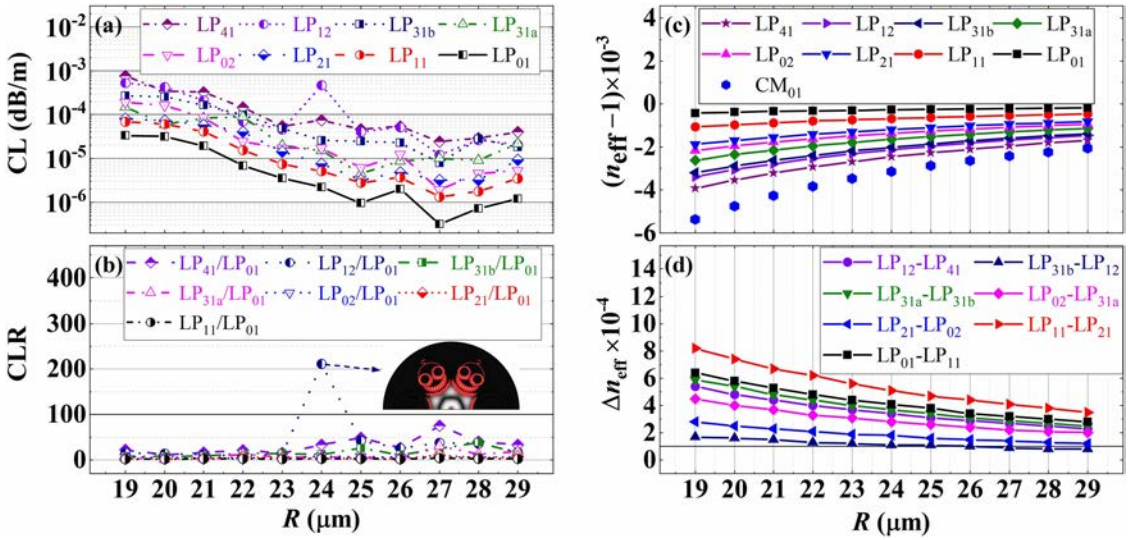

Fig. 8. Effects of the core radius on (a) CLs and (b) CLRs of the LP_{11}-LP_{41} modes; (c) n_{eff} curves of the LP_{01}-LP_{41} modes and cladding CM_{01} mode; (d) Δn_{eff} between adjacent modes of the HC-ARF for $N = 6$, $g = 1.50$ μm, $r_2 / r_1 = 0.70$, and $r_3 / r_2 = 0.40$ at 1550 nm. The electric field distribution of the LP_{41} mode (white) and the y-component of the Poynting vector (red) are shown in the inset in (b).

TABLE I
PARAMETERS OF THE OPTIMIZED FIBER DESIGN

Parameter	Value
N	6
g	1.5 μm
R	25 μm
r_2/r_1	0.70
r_3/r_2	0.40

26 μm, fluctuations are observed from the CLs of the LP_{01}-LP_{41} modes and the corresponding CLR curves. As shown in Fig. 8(c) and (d), the n_{eff} curves of the LP_{01}-LP_{41} modes are gradually close to each other as R increases, and Δn_{eff} between LP_{31b} mode and LP_{12} mode starts to be less than 1.0×10^{-4} when $R > 26$ μm. To satisfy the weak coupling condition, R is chosen to be 25 μm. In this case, the CLs of the LP_{01}-LP_{41} modes and CLRs of the LP_{11}-LP_{41} modes are less than 4.66×10^{-5} dB/m and 49, respectively.

F. Propagation Characteristics of Eight Modes

Based on our analysis described above, the optimized parameters are listed in Table I, and the unlisted r_1 is calculated by (2). Subsequently, the few-mode transmission characteristics are determined. When the wavelength changes from 1480 nm to 1670 nm, the CLs of the LP_{01}-LP_{41} modes are less than 1.72×10^{-4} dB/m, and the CLRs of LP_{11}-LP_{41} modes are all less than 100, as shown in Fig. 9. Hence, these eight modes can be transmitted efficiently by the few-mode HC-ARF. Moreover, the effective refractive index differences Δn_{eff} between adjacent modes are greater than 1.0×10^{-4}, which can effectively suppress the crosstalk between adjacent core modes.

The differential mode group delay (DMGD) is a key factor for few-mode fibers [24], and that between any two modes is described by the following equation [28]:

$$\mathrm{DMGD} = \frac{n_{\mathrm{eff}}^{(i)} - n_{\mathrm{eff}}^{(j)}}{c} - \frac{\lambda}{c}\left(\frac{dn_{\mathrm{eff}}^{(i)}}{d\lambda} - \frac{dn_{\mathrm{eff}}^{(j)}}{d\lambda}\right), \quad (4)$$

where c is the speed of light in vacuum, λ is the wavelength, and $n_{\mathrm{eff}}^{(i)}$ and $n_{\mathrm{eff}}^{(j)}$ are the effective refractive indexes of the i and j modes, respectively. Fig. 9(c) shows the DMGD of adjacent core modes at different wavelengths. The calculated results show that except for the LP_{31a}-LP_{02} mode, the DMGD of other adjacent modes increases with increasing wavelength, resembling the trend of the Δn_{eff} curve between adjacent core modes in Fig. 9(d). Since there are different n_{eff} changing rates relative to the wavelength for the LP_{31a} and LP_{12} modes, the DMGD of the LP_{31a}-LP_{02} modes diminishes slightly with increasing wavelength. Among the eight supported modes, the smallest DMGD appears between LP_{12} and LP_{31b} modes. The DMGD between the LP_{12} and LP_{31b} modes at 1480 nm is 0.38 ps/m, which is much larger than 0.10 ps/m, indicating that all the adjacent modes among the eight modes are well separated [23], [29]. All in all, this HC-ARF supports eight modes, including the LP_{01}-LP_{41} modes with large DMGDs, together with low CLs in the transmission bandwidth spanning wavelengths from 1480 nm to 1670 nm.

G. Bending Characteristics

Conformal mapping [30], [31] is applied to evaluate the effects of bending on the LP_{01}-LP_{41} modes. Because the power exchange caused by mode coupling is more likely to occur between the core and cladding modes [32], the x-direction is more sensitive to bending than the y-direction [24]. The parameter, BLR, defined as the ratio of the bending loss (BL) of the HOM to that of the LP_{01} mode (FM), is introduced to evaluate the

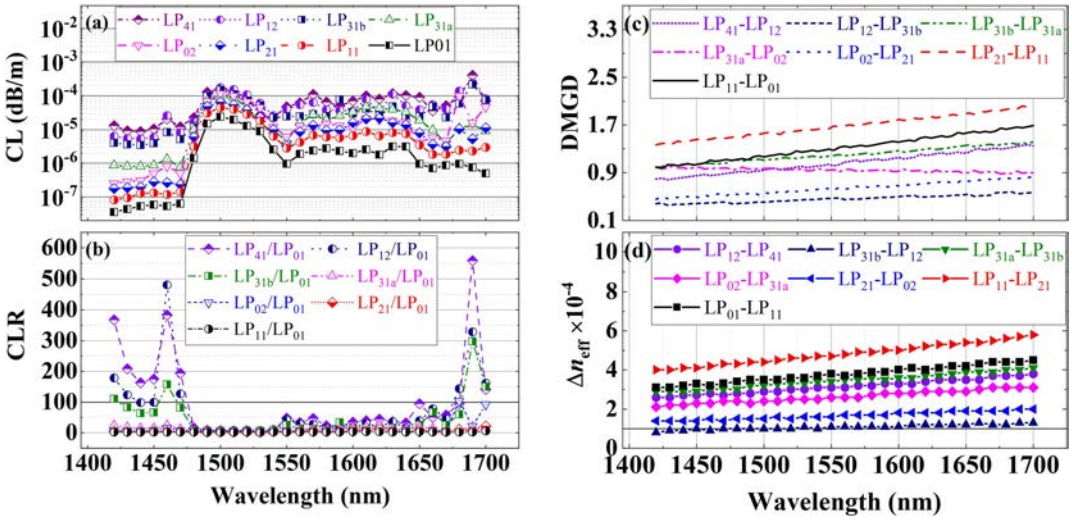

Fig. 9. (a) CLs and (b) CLRs of the LP_{01}-LP_{41} modes; (c) DMGD and (d) Δn_{eff} between adjacent modes in the LP_{01}-LP_{41} modes in the wavelength range between 1420 nm and 1700 nm of the HC-ARF for $N = 6$, $g = 1.50$ μm, $r_2 / r_1 = 0.70$, $r_3 / r_2 = 0.40$, and $R = 25$ μm.

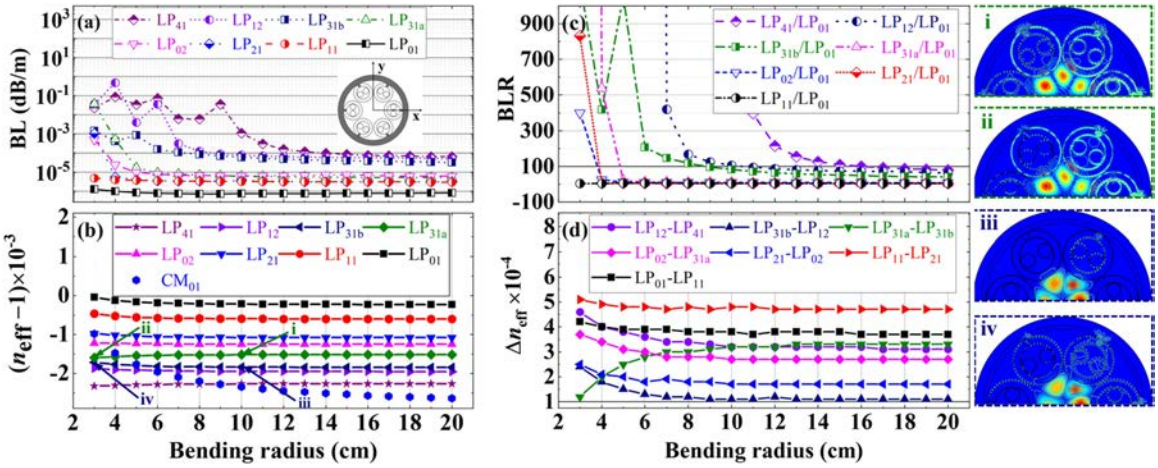

Fig. 10. Effects of the bending radius on (a) CLs of the LP_{01}-LP_{41} modes; (b) n_{eff} curves of the LP_{01}-LP_{41} modes and cladding CM_{01} mode; (c) BLRs of the LP_{11}-LP_{41} modes; (d) Δn_{eff} between adjacent modes in LP_{01}-LP_{41} modes of the HC-ARF for $N = 6$, $g = 1.50$ μm, $r_2 / r_1 = 0.70$, $r_3 / r_2 = 0.40$, and $R = 25$ μm at a wavelength of 1550 nm. The figures labeled i, ii, iii, and iv on the right panel correspond to the points marked as i, ii, iii, iv in (b) and represent the mode electric field distributions and field contours of the y-component of the LP_{31a} and LP_{31b} mode.

few-mode HC-ARF. When the BLR is less than 100, the HOM can be efficiently propagated in the few-mode fiber, even in the bent state.

When the bending radius is larger than 16 cm, the bending loss of the LP_{01}-LP_{41} modes is below 7.65×10^{-5} dB/m, while the BLR of the LP_{11}-LP_{41} modes is less than 100, as shown in Fig. 10(a) and (c). Fig. 10(d) shows that the crosstalk between adjacent core modes is suppressed because Δn_{eff} between adjacent modes of the LP_{01}-LP_{41} modes is greater than 1.0×10^{-4}, even if the bending radius is reduced to 3 cm. The n_{eff} curves in Fig. 10(b) show that the n_{eff} of the CM_{01} mode approaches that of the core modes and intersects the n_{eff} curves of the LP_{41}-LP_{01} modes when the bending radius is less than 10 cm, resulting in the loss peak shown in Fig. 10(a). Correspondingly, there is a sharp increase in the BLRs of the LP_{41}-LP_{11} modes and a decrease in the number of modes supported by the fiber, as shown in Fig. 10(c). Fig. 10(d) shows that Δn_{eff} between adjacent modes of the LP_{01}-LP_{41} modes increases if the bending radius is less than 7 cm, except Δn_{eff} between LP_{31a} and LP_{31b}, which decreases at a bending radius of less than 7 cm. This is because a smaller bending radius increases the degree of coupling of the core modes to the dielectric modes, except the LP_{31a} mode, which is coupled to the dielectric mode to a reduced degree, as shown in the right side inset in Fig. 10. In order to support eight weakly coupling modes more stably, the bending radius should be equal to or greater than 20 cm. When the bending radii are reduced to 5 cm and 3 cm, the fiber can still support five and two modes, respectively.

Fig. 11 presents the effects of bending on the transmission bandwidth for a radius of 20 cm. As shown in Fig. 11(a) and (b), the BLs of the LP_{01}-LP_{41} modes are less than 1.85×10^{-4} dB/m between 1480 nm and 1640 nm, while the BLRs of the LP_{11}-LP_{41} modes are less than 80. When the wavelength is longer than 1480 nm, Δn_{eff} between adjacent modes is larger

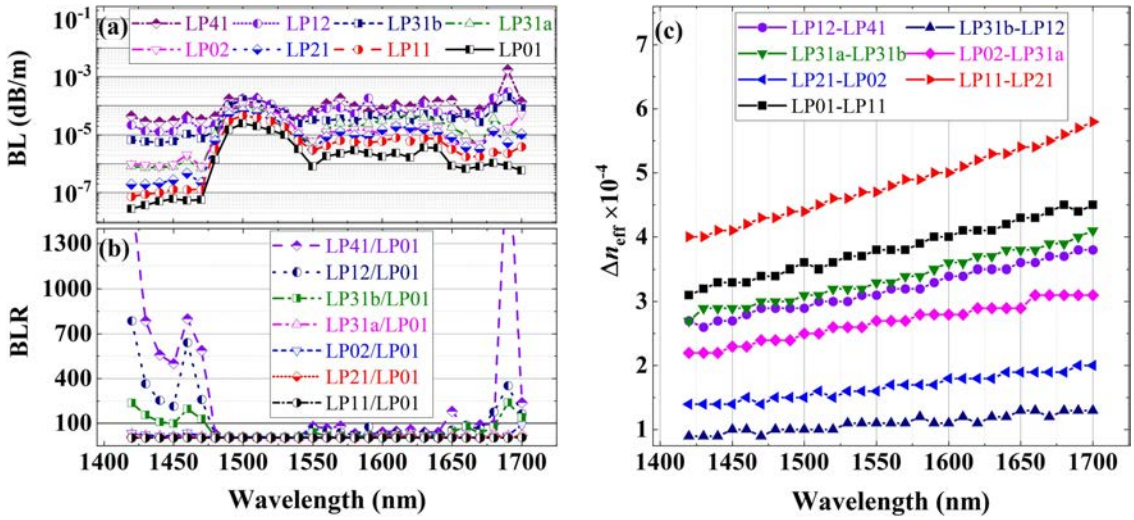

Fig. 11. (a) Variations of CLs and (b) BLRs of the LP_{01}-LP_{41} modes; (c) Δn_{eff} between adjacent modes for the LP_{01}-LP_{41} modes in the wavelength range between 1420 nm and 1700 nm of the HC-ARF for $N = 6$, $g = 1.50$ μm, $r_2 / r_1 = 0.70$, $r_3 / r_2 = 0.40$, and $R = 25$ μm subjected to a bending radius of 20 cm.

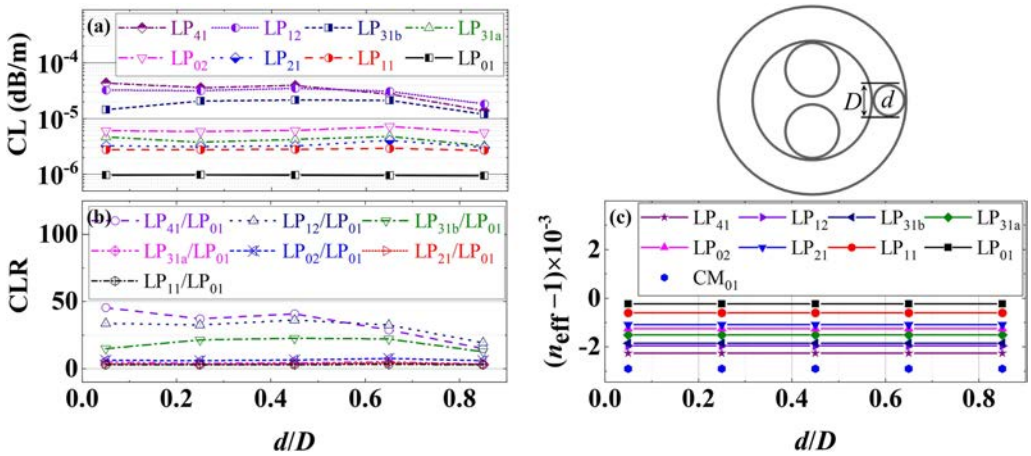

Fig. 12. Effects of the change of d / D on (a) CLs and (b) CLRs of the LP_{01}-LP_{41} modes; (c) n_{eff} curves of the LP_{01}-LP_{41} modes and cladding CM_{01} mode of the HC-ARF for $N = 6$, $g = 1.50$ μm, $r_2 / r_1 = 0.70$, $r_3 / r_2 = 0.40$, and $R = 25$ μm at 1550 nm.

than 1.0×10^{-4}, as shown in Fig. 11(c). Therefore, this ARF supports the LP_{01}-LP_{41} mode in the transmission band spanning the wavelength range from 1480 nm to 1640 nm for a bending radius of 20 cm with good few-mode transmission characteristics.

IV. Manufacturing Simplification and Tolerance Analysis

In order to reduce the fabrication difficulty, a silica rod is used in each cladding unit to support the middle tube. When the silica supporting rods of the cladding unit are changed to silica supporting tubes, the effects of the air duty ratio d / D on the CL and n_{eff} of the LP_{01}-LP_{41} modes are shown in Fig. 12. Fig. 12(a) and (b) show that a larger d / D of the supporting tube can reduce slightly CLs and CLRs of the LP_{31b}, LP_{12}, and LP_{41} modes. This is because a larger d / D reduces the coupling between these three modes and the modes of the silica rods. However, no matter how the d / D of the silica supporting tube is changed, there is no effect on n_{eff} of the LP_{01}-LP_{41} modes and CM_{01} mode, as shown in Fig. 12(c). Last but not least, in actual manufacturing, the use of silica rods simplifies pressure control during the drawing process and reduces the difficulty associated with fiber drawing.

Additionally, we also conduct an analysis of the manufacturing tolerance for the proposed few-mode HC-ARF. The manufacturing errors in HC-ARF primarily stem from fluctuations in the dimensions and wall thickness of nested tubes during fiber drawing process. The outermost nested tube's dimension r_1 is primarily determined by the variables g and R. Therefore, we focus on analyzing the tolerances of the key parameters including g, R, r_2, r_3. Since there is a slight effect of the small fluctuation of these parameters on CLs of eight core modes, we mainly investigate their effects on CLRs. In terms of the currently manufactured level of the HC-ARF, the $\pm 1\%$ fluctuation in the fiber geometric parameters can be guaranteed [33], and minimal changes in wall thickness t have negligible impact on the anti-resonant properties of the nested tube. On the basis of the optimal structure parameters, we have determined

TABLE II
CRITICAL PARAMETER TOLERANCE

Parameter	Tolerance	CLR
g	1.5 ± 6.7% μm	50.33-71.22
R	25 ± 2.4% μm	15.42-37.62
r_2	16.13 ± 2.9% μm	12.90-43.15
r_3	6.45 ± 5.0% μm	15.25-60.49

the appropriate tolerances by considering the maximum CLR below 100, as listed in Table II. It can be found that there are high fabrication tolerances for the proposed few-mode HC-ARF due to the fluctuations of the structure parameters during the fabrication process.

V. CONCLUSION

A weakly coupled nodeless few-mode HC-ARF is designed to support the propagation of eight modes, including the LP_{01}, LP_{11}, LP_{21}, LP_{02}, LP_{31a}, LP_{31b}, LP_{12}, and LP_{41} modes. The cladding structure is composed of six nodeless cladding units with three-layer nested tubes to restrain mode coupling between the LP_{01}-LP_{41} core modes and cladding mode while reducing the confinement loss of the LP_{01}-LP_{41} modes. The optimal nested tube size and core radius are determined by the finite element method. By adopting the optimized structural parameters of $N = 6$, $g = 1.50$ μm, $r_2 / r_1 = 0.70$, $r_3 / r_2 = 0.40$, and $R = 25$ μm, the CLs of the LP_{01}-LP_{41} modes are all less than 1.72×10^{-4} dB/m in the transmission bandwidth between 1480 nm and 1670 nm, while Δn_{eff} between adjacent modes is greater than 1.0×10^{-4}. All the corresponding DMGDs are greater than 0.38 ps/m. At a bending radius of 20 cm, the transmission characteristics are similar to those of a flat fiber, indicating stable transmission of the eight weakly coupled modes. When the bending radii decrease to 5 cm and 3 cm, the fiber still supports five and two modes, respectively. Owing to the merits such as small loss and low crosstalk of the eight guided modes, the fiber has large potential in short-distance and high-capacity data transmission applications for data centers.

REFERENCES

[1] K. Saitoh and S. Matsuo, "Multicore fiber technology," *J. Lightw. Technol.*, vol. 34, no. 1, pp. 55–66, Jan. 2016.

[2] M. Zahidy et al., "Practical high-dimensional quantum key distribution protocol over deployed multicore fiber," *Nat. Commun.*, vol. 15, no. 1, Feb. 2024, Art. no. 1651.

[3] M. Bigot, M. Bsaibes, L. Bigot, Y. Quiquempois, and P. Sillard, "Few-mode fibers: Characterizations and applications," in *Proc. Opt. Fiber Commun. Conf. Exhib.*, 2023, pp. 1–3.

[4] B. J. Puttnam, G. Rademacher, and R. S. Luís, "Space-division multiplexing for optical fiber communications," *Optica*, vol. 8, no. 9, Sep. 2021, Art. no. 1186.

[5] A. D. Ellis, N. M. Suibhne, D. Saad, and D. N. Payne, "Communication networks beyond the capacity crunch," *Philos. Trans. Roy. Soc. A.*, vol. 374, no. 2062, Mar. 2016, Art. no. 20150191.

[6] P. P. Mitra and J. B. Stark, "Nonlinear limits to the information capacity of optical fibre communications," *Nature*, vol. 411, no. 6841, pp. 1027–1030, Jun. 2001.

[7] Y. Y. Wang, N. V. Wheeler, F. Couny, P. J. Roberts, and F. Benabid, "Low loss broadband transmission in hypocycloid-core Kagome hollow-core photonic crystal fiber," *Opt. Lett.*, vol. 36, no. 5, pp. 669–671, Mar. 2011.

[8] Y. Chen et al., "Hollow core DNANF optical fiber with <0.11 dB/km loss," Presented at Opt. Fiber Commun. Conf., San Diego, CA, USA, Mar. 24–28, 2024, Paper Th4A.8.

[9] S. Johnson et al., "Low-loss asymptotically single-mode propagation in large-core OmniGuide fibers," *Opt. Exp.*, vol. 9, no. 13, pp. 748–779, Dec. 2001.

[10] P. Russell, "Photonic crystal fibers," *Science*, vol. 299, no. 5605, pp. 358–362, Jan. 2003.

[11] G. J. Pearce, G. S. Wiederhecker, C. G. Poulton, S. Burger, and P. S. Russell, "Models for guidance in Kagome-structured hollow-core photonic crystal fibres," *Opt. Exp.*, vol. 15, no. 20, 2007, Art. no. 12680.

[12] A. N. Kolyadin, A. F. Kosolapov, A. D. Pryamikov, A. S. Biriukov, V. G. Plotnichenko, and E. M. Dianov, "Light transmission in negative curvature hollow core fiber in extremely high material loss region," *Opt. Exp.*, vol. 21, no. 8, Apr. 2013, Art. no. 9514.

[13] F. Yu and J. C. Knight, "Spectral attenuation limits of silica hollow core negative curvature fiber," *Opt. Exp.*, vol. 21, no. 18, Sep. 2013, Art. no. 21466.

[14] P. J. Roberts et al., "Ultimate low loss of hollow-core photonic crystal fibres," *Opt. Exp.*, vol. 13, no. 1, pp. 236–244, 2005.

[15] F. Poletti, "Nested antiresonant nodeless hollow core fiber," *Opt. Exp.*, vol. 22, no. 20, Oct. 2014, Art. no. 23807.

[16] C. Wei, R. Joseph Weiblen, C. R. Menyuk, and J. Hu, "Negative curvature fibers," *Adv. Opt. Photon.*, vol. 9, no. 3, pp. 504–561, Sep. 2017.

[17] K.-I. Kitayama and N.-P. Diamantopoulos, "Few-mode optical fibers: Original motivation and recent progress," *IEEE Commun. Mag.*, vol. 55, no. 8, pp. 163–169, Aug. 2017.

[18] C. Goel and S. Yoo, "Multimode nested antiresonant hollow core fiber," *J. Lightw. Technol.*, vol. 39, no. 20, pp. 6592–6598, Oct. 2021.

[19] W. Shere, E. N. Fokoua, G. T. Jasion, and F. Poletti, "Designing multi-mode anti-resonant hollow-core fibers for industrial laser power delivery," *Opt. Exp.*, vol. 30, no. 22, pp. 40425–40440, Oct. 2022.

[20] M. Al Mahfuz and M. S. Habib, "Enhanced inhibited mode-coupling: Multi-mode hollow-core anti-resonant fiber designs," *IEEE J. Sel. Top. Quantum Electron.*, vol. 30, no. 6, Nov./Dec. 2024, Art. no. 4301409.

[21] W. Shere, G. T. Jasion, E. Numkam Fokoua, and F. Poletti, "Low loss, large bandwidth antiresonant hollow-core fiber design for short-reach links," in *Proc. Opt. Fiber Commun. Conf. Exhib.*, 2020, pp. 1–3.

[22] L. Wang and S. LaRochelle, "Design of eight-mode polarization-maintaining few-mode fiber for multiple-input multiple-output-free spatial division multiplexing," *Opt. Lett.*, vol. 40, no. 24, pp. 5846–5849, Dec. 2015.

[23] Z. Wang, J. Tu, Z. Liu, C. Yu, and C. Lu, "Design of weakly coupled two-mode hollow-core antiresonant fiber with low loss," *J. Lightw. Technol.*, vol. 38, no. 4, pp. 864–874, Feb. 2020.

[24] H. Liu et al., "Low bending loss few-mode hollow-core anti-resonant fiber with glass-sheet conjoined nested tubes," *Opt. Exp.*, vol. 30, no. 12, pp. 21833–21842, Jun. 2022.

[25] M. S. Habib, J. E. Antonio-Lopez, C. Markos, A. Schülzgen, and R. Amezcua-Correa, "Single-mode, low loss hollow-core anti-resonant fiber designs," *Opt. Exp.*, vol. 27, no. 4, pp. 3824–3836, Feb. 2019.

[26] I. H. Malitson, "Interspecimen comparison of the refractive index of fused silica," *J. Opt. Soc. Amer.*, vol. 55, no. 10, pp. 1205–1209, Oct. 1965.

[27] T. P. White et al., "Multipole method for microstructured optical fibers I formulation," *J. Opt. Soc. Amer. B*, vol. 19, no. 10, pp. 2322–2330, Oct. 2002.

[28] Y. Wu and K. S. Chiang, "Compact three-core fibers with ultra-low differential group delays for broadband mode-division multiplexing," *Opt. Exp.*, vol. 23, no. 16, pp. 20867–20875, Aug. 2015.

[29] P. Sillard, M. Bigot-Astruc, D. Boivin, H. Maerten, and L. Provost, "Few-mode fiber for uncoupled mode-division multiplexing transmissions," in *Proc. 37th Eur. Conf. Exhib. Opt. Commun.*, 2011, pp. 1–3.

[30] M. Heiblum and J. Harris, "Analysis of curved optical waveguides by conformal transformation," *IEEE J. Quantum Electron .*, vol. JQE-11, no. 2, pp. 75–83, Feb. 1975.

[31] Y. Wang and W. Chang, "Multi-nested antiresonant hollow-core fiber with ultralow loss and single-mode guidance," *Opt. Exp.*, vol. 31, no. 11, pp. 18250–18264, May 2023.

[32] W. Belardi and J. C. Knight, "Hollow antiresonant fibers with low bending loss," *Opt. Exp.*, vol. 22, no. 8, pp. 10091–10096, Apr. 2014.

[33] G. T. Jasion et al., "Hollow core NANF with 0.28 dB/km attenuation in the C and L bands," in *Proc. Opt. Fiber Commun. Conf. Exhib.*, 2020, pp. 1–3.